A review of breast tomosynthesis. Part I. The image acquisition process

Ioannis Sechopoulos[a)]
Department of Radiology and Imaging Sciences, Hematology and Medical Oncology and Winship Cancer Institute, Emory University, 1701 Upper Gate Drive Northeast, Suite 5018, Atlanta, Georgia 30322

(Received 13 June 2012; revised 16 November 2012; accepted for publication 16 November 2012; published 4 January 2013)

Mammography is a very well-established imaging modality for the early detection and diagnosis of breast cancer. However, since the introduction of digital imaging to the realm of radiology, more advanced, and especially tomographic imaging methods have been made possible. One of these methods, breast tomosynthesis, has finally been introduced to the clinic for routine everyday use, with potential to in the future replace mammography for screening for breast cancer. In this two part paper, the extensive research performed during the development of breast tomosynthesis is reviewed, with a focus on the research addressing the medical physics aspects of this imaging modality. This first paper will review the research performed on the issues relevant to the image acquisition process, including system design, optimization of geometry and technique, x-ray scatter, and radiation dose. The companion to this paper will review all other aspects of breast tomosynthesis imaging, including the reconstruction process. © *2013 American Association of Physicists in Medicine*. [http://dx.doi.org/10.1118/1.4770279]

Key words: breast tomosynthesis, digital mammography, breast cancer, review, image acquisition, x-ray scatter, acquisition geometry, radiation dose

I. INTRODUCTION

Standard mammography is a low cost, fast, noninvasive x-ray study that involves relatively low doses of ionizing radiation. However, the two-dimensional (2D) nature of mammography results in tissue superposition, which can create two problems: dense glandular tissue located above and/or below a lesion of interest can reduce the visibility of the lesion (reducing sensitivity), or two or more normal features that are only vertically separated can appear to be the projection of a lesion of interest (reducing specificity). These two phenomena are partially responsible for a sensitivity and specificity of screening mammography of 83.5% and 90.9%, respectively.[1] These values may be lower for women with dense breasts.[2,3]

The introduction of digital acquisition has helped improve mammography by avoiding screen-film's narrow range of linear response, among other issues. However, digital mammography still only acquires a 2D projection of a three-dimensional (3D) object, maintaining the issue of tissue superposition. Potentially, the most important contribution of digital mammography is its flexibility, which allows for the development of imaging methods that can resolve some of the limitations of mammography. Specifically, to overcome the loss of information in the third dimension, among other advantages, two new imaging methods have been developed: dedicated breast computed tomography[4–10] and tomosynthesis imaging of the breast. While dedicated breast CT remains promising, breast tomosynthesis is now clinical technology, with different systems having received approval for clinical use around the world and one system being approved in the U.S. over the last few years (see Table I).

Tomosynthesis is a technique that enables pseudotomographic imaging by acquiring a limited number of projections from a narrow angular range, and combining these projections to reconstruct a quasi-3D image. An in-depth discussion of the history of the development of tomosynthesis has been published by Dobbins and Godfrey[11] and Dobbins.[12]

In tomosynthesis imaging of the breast, first demonstrated by Niklason *et al.* in 1997,[13] the acquisition geometry is very similar to that used in mammography, with the difference that the x-ray tube is rotated in one plane around the static compressed breast and a series of images is acquired, one at each x-ray tube position (Fig. 1). During the acquisitions, the detector can either be static or rotate to maintain its top surface normal to the x-ray tube.[14,15] The series of projections acquired is then processed by a reconstruction algorithm which uses the different location in the projections of the same tissues to compute their vertical position, thereby estimating the 3D distribution of the tissues. Due to the limited angle of the projection acquisitions, tomosynthesis is characterized by anisotropic spatial resolution, with very high spatial resolution in the planes parallel to the detector, and a considerably lower resolution in the perpendicular direction. However, this low spatial resolution in the depth direction is deemed to be enough to substantially reduce the issue of tissue superposition, lowering its impact on sensitivity and specificity.

This two part review of digital breast tomosynthesis (DBT) will concentrate on the medical physics-related aspects of the research performed to date. This paper will review the image acquisition aspects of DBT, while its companion paper will address all the postacquisition aspects, including image reconstruction. The investigation of the clinical performance of DBT and its comparison to mammography is beyond the scope of this review, but has been covered in depth in a review by Baker and Lo.[16]

TABLE I. Characteristics of breast tomosynthesis systems in clinical use or under development. The specifications for these systems, especially the prototypes, could change in the future.

System	GE Essential	Hologic Selenia Dimensions	IMS Giotto TOMO	Philips MicroDose	Planmed Nuance Excel DBT	Siemens MAMMOMAT Inspiration
Detector type	Full field—indirect	Full field—direct (a-Se)	Full field—direct (a-Se)	Linear slit scan–spectral photon counting (Si)	Full field—direct (a-Se)	Full field—direct (a-Se)
Detector size (cm)	24 × 30	24 × 29	24 × 30	21 line detectors, each 24 cm long	24 × 30	24 × 30
Detector pixel size (μm)	100	70 (binned 2 × 2)[a]	85	50 (perpendicular to motion)	85	85
Detector motion	Static	Rotating	Static	Continuous slit scan	Rotating during exposure[b]	Static
X-ray tube target	Mo or Rh	W	W	W	W	W
X-ray tube filtration	0.03 mm Mo or 0.025 mm Rh	0.7 mm Al	0.05 mm Rh or 0.05 mm Ag	0.5 mm Al	0.075 mm Ag or 0.06 mm Rh	0.05 mm Rh
X-ray tube motion	Step-and-shoot	Continuous	Step-and-shoot	Continuous	Continuous	Continuous
Angular range (deg)	25	15[c]	40	11	30	50[d]
Number of projections	9	15	13[e]	21	15	25
Scan time (s)	7	3.7	12	3–10	20	25[d]
Source to detector distance (cm)	66	70	68	66	65	65.5
Detector to center of rotation distance[f] (cm)	4	0	2	−40	4.37	4.7
Air gap (cm)	2.2	2.5	2.2	0.4–2.4	2.38	1.7
Reconstruction method	Iterative	FBP	Iterative with total variation regularization	Iterative	Iterative	FBP
Development stage[g]	Prototype	Commercial system	Commercial system[h]	Prototype	Prototype	Commercial system[h]
References	16,31	16	32–35	26,27,36	37	16,38–40

[a]Reconstruction results in an in-plane pixel size of approximately 100 μm.
[b]Detector and compressed breast are rotated with x-ray source, while each projection is being acquired (x-ray tube current is on). Detector and breast are returned to original position at end of each projection.
[c]This system supports an angular range up to 30°, which requires a software change by the manufacturer.
[d]These values for angular range and scan time are for the x-ray tube motion; the x-ray exposures actually cover ~46° in 20 s.
[e]In the current commercial system outside the U.S., this system can be set to use 50% of the total tube output for the 0° projection and the rest distributed evenly among the other 12 projections.
[f]Positive values are towards the x-ray source.
[g]For systems which perform both mammography and DBT, this information is specific for the DBT mode.
[h]Currently not approved for clinical use in the U.S. by the FDA.

II. HARDWARE

II.A. General system design

Currently, most DBT systems consist of the same basic components as digital mammography systems: a direct or indirect full field digital detector, a breast support and compression plate, and an x-ray tube mounted on an arm. The single basic hardware addition that transforms a mammography system into a tomosynthesis system is the ability of the x-ray tube to rotate around a point close to or on the detector and having a detector with relatively fast readout. Of course, additional modifications have been implemented by manufacturers to optimize their system's tomosynthesis acquisition compared to the mammography acquisition, including, for example, different x-ray spectrum filtration and pixel binning.[17]

Some tomosynthesis systems being developed diverge from this more "traditional" design. For example, to avoid focal spot blurring due to the x-ray tube motion during acquisition[18] and potentially shorten total acquisition time, a carbon nanotube array of x-ray sources is being investigated as a replacement for the x-ray tube and rotating gantry.[19–25] In recent work, the investigators replaced the x-ray tube and gantry of a commercial DBT system (Selenia Dimensions, Hologic, Inc., Bedford, MA) with a carbon nanotube array with 31 x-ray sources, spanning 370 mm, resulting in an angular coverage of 30°. The stationary x-ray source was shown to yield an improved modulation transfer function (MTF)

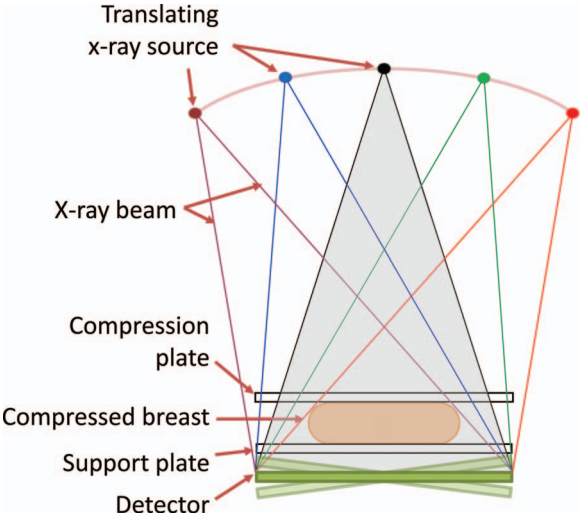

FIG. 1. Schematic of a breast tomosynthesis acquisition, in which a number of projection images is acquired of the compressed breast, while the x-ray source rotates around a center of rotation close or on the detector surface while the detector is either static or rotates, depending on the system design.

compared to that with a standard rotating x-ray tube, in addition to an increase in the sharpness of phantom microcalcification images. Detector readout rate and x-ray tube current and exposure time are issues that still need to be addressed to optimize total scan time.[25]

Another tomosynthesis system that fundamentally differs from the "traditional" full-field design is one based on a scanning slit photon counting detector (Sectra Microdose, now Philips Healthcare, Best, The Netherlands). In this system, a multislit linear detector and a collimated x-ray fan beam are scanned in an arc across the breast with the center of rotation below the breast.[26,27] Advantages of this system include a very low scatter signal,[28] no electronic noise, and high quantum efficiency. This results in a highly efficient system with low radiation dose requirements. In addition, a new version of this photon counting detector includes energy resolution, allowing for simultaneous acquisition of two images (low and high energies).[26] However, due to the system's acquisition geometry, this tomosynthesis system cannot acquire mammographic images. A similar slot scanning photon counting system with a linear motion has been investigated, but its development has been discontinued.[29,30]

Table I summarizes the characteristics of the different tomosynthesis systems currently in clinical or preclinical use.

II.B. Detectors

Extensive work has been performed to optimize the detectors for tomosynthesis imaging. In addition to the requirements for digital mammography, detectors for DBT need to achieve additional capabilities. These include: (i) faster reading time, to keep the total acquisition time of all projections to a minimum, with (ii) minimal ghosting and lag, which has been shown to introduce image artifacts,[41] and (iii) minimal reduction in detective quantum efficiency (DQE) at low exposures (given the need to divide the total exposure over several projections).

Various studies have characterized the capabilities of direct detectors based on an amorphous selenium (a-Se) layer for direct conversion from x-rays to electron-hole pairs. Bissonnette *et al.* characterized a mammography system modified for DBT imaging (Siemens Novation DR) using both a 2 × 1 binned (binning in the x-ray tube travel direction) and a full resolution non-binned readout mode.[42] As expected, binned mode results in an increase in signal-to-noise ratio (SNR), but with a penalty in the MTF in the binning direction (parallel to the x-ray source motion). Reduction in DQE with decreasing exposure, although relatively low for the full resolution mode, is further diminished for the binned mode. In a subsequent empirical investigation again using a Siemens mammography system modified for DBT, Zhao and Zhao measured the MTF with the x-ray tube in motion, replicating the acquisition conditions for operating with a continuous motion system. It was determined that 2 × 1 pixel binning has a larger impact on the MTF than the blurring due to the motion of the focal spot.[43] On the other hand, lag was found to be higher when the detector is binned, while ghosting is minimal in both modes. It was also found that the DQE at the lowest exposure levels relevant to DBT decreases only by about 20% compared to the high exposure condition.

Reporting on the development of a different a-Se based direct detector for the Hologic DBT system, Cheung *et al.* characterized a new detector optimized for DBT that reduces the reading cycle time by replacing the dielectric/Se layer at the top of the Se surface with a charge conductive layer.[44] This modification eliminates a major location of charge trapping, which required an additional erase cycle in between image acquisitions and extended the readout cycle time. This change, in addition to the use of 2 × 2 pixel binning, allowed for a decrease in readout time to the subsecond level with minimal ghosting, resulting in a total scan time for a complete tomosynthesis acquisition of 3.7 s in the final system.[17]

II.C. X-ray incidence angle impact on detection

In DBT systems where the detector remains stationary, the incidence angle of the x-rays onto the detector can be large. The consequences of this large incidence angle on the point spread function (PSF) and the MTF have been studied empirically,[43,45] analytically,[43,45–48] and using Monte Carlo simulations[49] for both direct a-Se detectors and scintillator-based indirect detectors. The effect on the PSF in indirect detectors was first studied using Monte Carlo methods by Badano *et al.*, showing the anisotropy introduced by the non-normal incidence and its variation throughout the detector surface due to the varying incidence angle.[49] On follow-up work, Freed *et al.* developed an analytical model to predict the PSF, again for indirect detectors, for different conditions without having to perform CPU-intensive Monte Carlo simulations.[46] This model was then extended by the same group to include direct detectors.[50] As expected given the variation in the PSF, the impact of the oblique incidence on the MTF was also found to be substantial for both direct and indirect detectors. In empirical and analytical work, the MTF was found to be reduced by 25% to 30% at 6 lp/mm.[43,45] Reiser *et al.*

found that oblique incidence on indirect detectors results in a loss of DQE at high frequencies and a small increase at low frequencies, with a 13% loss in detectability for small signals.[51] Acciavatti and Maidment derived the MTF and noise power spectra (NPS) and estimated the DQE from first principles for indirect detectors with unstructured scintillators, such as gadolinium oxysulfide doped with terbium (Gd_2O_2S:Tb).[47,48] The authors used their analytical model to study the dependence of these metrics on x-ray incidence angle and on detector design. They found that the response of back-illuminated detectors is less sensitive to incidence angle than that of front-illuminated detectors, and would therefore be more suitable for tomosynthesis imaging. Currently there are no back-screen detectors available, but ongoing technology developments may result in the introduction of this type of detector in the future.

II.D. Other detector designs

In early work, the development of a-Se-based photon counting detectors was investigated by Chen *et al.* by developing a theoretical model and validating it empirically with a one dimensional detector prototype.[52] Promising results were found by the authors, showing that this type of detector is feasible. Naday *et al.* characterized a CMOS-based detector specifically designed for DBT, which allows for variable binning and gain for each acquisition.[53]

III. GEOMETRY OPTIMIZATION

As with most medical imaging modalities, acquisition of a DBT image involves the selection of a number of parameters. In DBT, the acquisition parameters that have resulted in the most research are those involved in defining the acquisition geometry, specifically the number of projections, the total angular range covered by the projections, and the distribution of the projections. The reason for the high interest in these parameters is twofold: these parameters have a high impact on the resulting image quality, and there are no previously established modalities that involve similar parameters from which to draw any experience. This latter reason is why although technique optimization (e.g., tube voltage) has also been studied, the availability of previous experience from digital mammography has made this an easier problem to address. The vast differences in the geometrical parameter values used in current tomosynthesis systems, as shown in Table I, are a prime example of the complexity involved in optimizing these parameters. *A priori*, it would be expected that maximizing the number of projections and the angular range would result in the highest image quality. However, the ability to maximize the number of projections is constrained by limits on the total exposure available for all projections. This is because a higher number of projections require the lowering of the exposure per projection, increasing quantum noise in each and potentially making electronic noise more dominant. Increasing the angular range also results in higher obliquity in incidence angle, which, as discussed earlier, results in a degradation of the spatial resolution. Finally, the possibility of having an irregular distribution of the projection angles throughout the angular range and/or using different tube current-exposure time products for different projection angles adds to the complexity of the optimization problem. But it could also result in an increase in image quality, especially for specific clinical tasks (e.g., microcalcification vs soft tissue lesion detection).[54,55]

To study the optimal values for the geometrical parameters relevant to DBT imaging, Maidment *et al.* performed simulations of tomosynthesis imaging of a wire and imaged a rabbit with a photon counting tomosynthesis system.[29] The wire simulations were performed without the addition of noise and it was found that maximizing the angular range and the number of projections yields the optimal acquisition protocol. Studying the effect of the number of projections included in the tomosynthesis set but this time using clinical images, Maidment *et al.* again found that maximizing the number of projections yields better image quality.[30] In the rabbit images of the first work and in the patient images of this last work, the authors introduced the additional noise expected due to the increase in the total number of projections after reconstruction. Using a homogeneous phantom, Ren *et al.* found that increasing the number of projections for a fixed total dose and angular range results in a small improvement of the vertical profile of contrast-to-noise ratio (CNR) for larger microcalcifications, making no difference for smaller calcifications, while in-plane image quality is degraded with increasing number of projections.[56] Zhou *et al.* performed a simulation-based study comparing four different acquisition protocols (a fifth variation involved the use of 2×2 pixel binning) using a monochromatic x-ray beam and a homogeneous background and three different reconstruction methods.[18] As a metric of in-plane image quality, the authors used the signal-difference-to-noise ratio, while for vertical resolution, the authors used a common metric in tomosynthesis imaging, the artifact spread function (ASF), which was defined by Wu *et al.*[57] as

$$\mathrm{ASF}(z) = \frac{I_s(z) - I_{BG}(z)}{I_s(z_0) - I_{BG}(z_0)}, \tag{1}$$

where z_0 is the location of the in-focus plane, z is the current location, I_s is the mean pixel value of the signal, and I_{BG} is the mean pixel value of the background. Using these metrics, Zhou *et al.* found that maximizing angular range and number of projections results in the best image quality.

Hu *et al.* developed and validated a cascaded linear systems model of tomosynthesis acquisition and then used it to predict the PSF and ASF of a small high contrast object for varying angular ranges.[58] The authors found, as expected, that an increased angular range results in a narrower vertical PSF. However, they also found from their analysis of the ASF, that an increase in angular range should be accompanied by an increase in the number of projections, to minimize the presence of ghosting of high contrast objects located in off-focus planes, which are manifested by an increase in the tails of the ASF. The need for an increase in the minimum number of projections when increasing the angular range to minimize the introduction of reconstruction artifacts was also reported by Mertelmeier *et al.*[59]

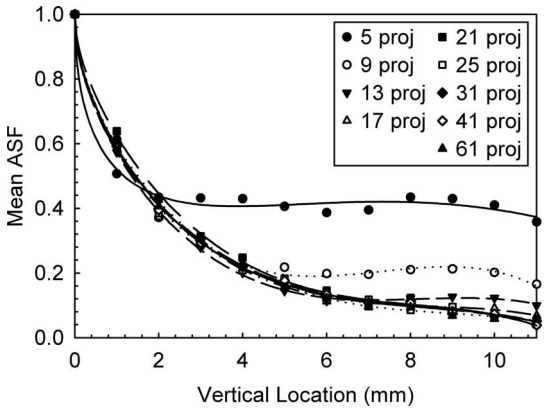

FIG. 2. Artifact spread function from simulated DBT images acquired with a 60° angular range and varying number of projections. Reprinted with permission from I. Sechopoulos and C. Ghetti, "Optimization of the acquisition geometry in digital tomosynthesis of the breast," Med. Phys. **36**(4), 1199–1207 (2009). Copyright © 2009, American Association of Physicists in Medicine (AAPM).

This was also confirmed by Sechopoulos and Ghetti, who in addition found that increasing the number of projections for each angular range beyond that required to minimize the off-focus plane artifacts does not result in any further improvement in the vertical resolution (Fig. 2).[59] The authors further found that the in-plane image quality is inversely proportional to the number of projections under a constant dose condition. Therefore, the upper limit in vertical resolution is given by the angular range, and the number of projections for a specific angular range should be that which just meets the required "threshold" number to obtain the best possible ASF, with no benefit in a further increase. To investigate these relationships, the authors proposed the "quality factor," a combination of the in-plane image quality and the vertical resolution, as a metric to compare tomosynthesis image quality, defined as

$$\mathrm{QF} = \frac{\mathrm{CNR}}{\mathrm{ASF}_W}, \tag{2}$$

where the CNR provides the metric for in-plane image quality, and the $\mathrm{ASF_w}$ is a measure of the width of the ASF, e.g., the z location at which the ASF(z) attains a value of 0.2. This threshold value was used because visual inspection of the ASF curves showed that noise started being dominant at values below this level. Of the 63 different combinations of geometrical acquisition parameters investigated, Sechopoulos and Ghetti found that the highest image quality was obtained with a 60° angular range (the widest they investigated) and 13 projections. As can be seen from Fig. 2, the number of projection angles required to achieve the "threshold" beyond which the vertical resolution is not further improved for a specific angular range is quite low. Using the same QF metric, Tucker *et al.* arrived at similar conclusions on the impact of angular range and number of projections for DBT performed with stationary carbon nanotube x-ray sources.[24]

Using a more advanced image quality metric, specifically the detectability of a simulated lesion as evaluated by an observer model, Chawla *et al.* also studied the impact of total angular range and number of projections on tomosynthesis image quality, analyzing both the projections and the reconstructed images.[61,61] Under the constant total dose condition, the results agree with the findings of Sechopoulos and Ghetti; detectability increases with increasing angular range and number of projections, but the latter achieves a maximum beyond which observer performance decreases. Of the parameter values studied, Chawla *et al.* found that the maximum angular range studied (44.8°) and 15–17 projections resulted in the maximum lesion detectability. Using numerical observers that included search, Gifford *et al.* found that for one task [background-known-exactly (BKE)], fewer projections and wider angular range was beneficial, while for the quasi-BKE task a higher number of projections showed an improving trend.[63]

In a study that investigated the effect of lesion size on the optimization of geometrical acquisition parameters, Reiser and Nishikawa, using an observer model with simulated breast backgrounds and lesions, found that larger lesion detectability is insensitive to the number of projections and to quantum noise.[64] For smaller lesions at higher quantum noise levels, the previous results reporting a "threshold" number of projections for a given angular range were confirmed. Finally, Reiser and Nishikawa also found that increasing the angular range improves detectability for all lesion sizes.

In a study using both a breast phantom and three human subjects, Lu *et al.* investigated both varying angular range and varying angular distribution for a fixed number of projections.[65] For this, the authors compared the CNR, the in-plane full width at half maximum (FWHM) and the ASF of microcalcifications for each acquisition parameter set. As expected, the acquisitions with a larger angular range resulted in an improved ASF. In addition, the acquisitions that involved a larger number of projections at the widest angles also resulted in an improved ASF, while the acquisitions with very narrow angles or with most projections concentrated in the center angles resulted in artifacts. The in-plane FWHM variability with acquisition conditions depended on the direction of the profile, with the FWHM in the direction perpendicular to tube motion being insensitive to acquisition condition, while in the other direction the FWHM was improved with narrower acquisitions. Finally, the authors found that the CNR for small subtle microcalcifications was also improved for narrower acquisitions, while for larger microcalcifications the CNR did not vary with acquisition conditions. In agreement with most of these studies, Van de Sompel *et al.* found that when the total dose used for acquisition remains constant, image quality continuously improves with wider angular range but that a maximum is reached at a certain number of projections, after which image quality declines.[66] For their analysis, Van de Sompel *et al.* used both CNR and a numerical observer in a very comprehensive analysis of various aspects affecting image quality of DBT reconstructions. As part of this study, the authors also compared using a static vs rotating detector acquisition geometry, and found that the rotating detector results in an improved CNR, especially for the filtered backprojection (FBP) and maximum likelihood (ML) reconstruction algorithms, but in a slight decrease in performance of the numerical observer. Ren *et al.*, however, suggested that CNR

alone is not an appropriate metric for optimization of angular range, since a variation in angular range affects the inherent filtration performed by the reconstruction algorithm, which in turn impacts the value of CNR, rather than the angular range variation having a direct impact on CNR.[67]

Finally, Gang *et al.* proposed an analysis framework for optimization of geometry parameters using cascaded systems analysis by measuring the background power spectra of textured phantoms and incorporating this feature into a generalized detectability model that takes into account background, quantum and electronic noise.[68] The authors used this model to investigate the impact of varying angular range and number of projections (including values relevant to tomosynthesis and CT) on signals of different frequency characteristics, and found that the optimal parameter values differ for low and high frequency tasks.

III.A. Alternative x-ray source motion

In standard tomosynthesis designs, the x-ray source moves in one plane on an arc around the imaged breast, as shown in Fig. 1. However, other designs for DBT have been proposed. Stevens *et al.*[69] proposed circular tomosynthesis, in which the x-ray source and detector move in circles in planes parallel to each other. Zeng *et al.* proposed to combine the acquisition of a CT scan with a tomosynthesis acquisition to result in improved reconstruction quality by combining a low resolution CT scan acquired using an arc-and-line motion with a high resolution tomosynthesis scan acquired using a conventional arc motion.[70] Xia *et al.* proposed moving the x-ray source in two arcs normal to each other, therefore encompassing a portion of a spherical surface above the imaged object.[71] This geometry, with the addition of combining the source rotation with rotation of the detector, was also proposed by Zhang and Yu, who also presented a different way of covering this spherical surface: a sequence of curved zigzag lines (Fig. 3).[72] Both of these designs aim to sample the frequency domain more completely, resulting in improved image quality. All these proposals have been tested using either phantoms or computer simulations. Although their results are encouraging, potential geometrical issues with the rest of the patient's body would need to be addressed for these geometries to be successful clinically.

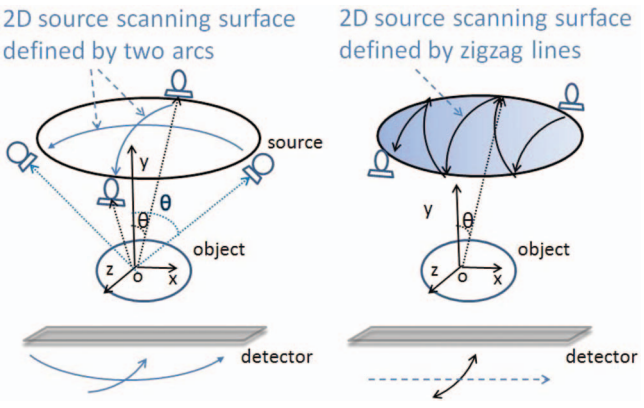

FIG. 3. Alternative x-ray source motions proposed by Zhang and Yu for acquisition of tomosynthesis projections Ref. 72. Reprinted with permission from J. Zhang and C. Yu, "A novel solid-angle tomosynthesis (SAT) scanning scheme," Med. Phys. **37**(8), 4186–4192 (2010). Copyright © 2010, American Association of Physicists in Medicine.

IV. TECHNIQUE OPTIMIZATION

Although the optimization of acquisition technique parameters for DBT could be deemed simpler than the optimization of the geometrical acquisition parameters due to the prior knowledge available from digital mammography, the optimal techniques, especially tube voltage selection, could differ greatly due to the reduction in anatomical noise inherent in tomosynthesis imaging compared to planar imaging. In addition, the acquisition of multiple projections during a complete tomosynthesis acquisition introduces the question of how the total exposure available for the complete study should be divided among the projections. These are the two main aspects that have been addressed by the studies reported on technique optimization.

IV.A. Tube voltage optimization

Investigating the optimal tube voltage for use in DBT, Ren *et al.* reported on an experimental x-ray spectrum optimization study that used a homogeneous background, x-ray spectra with a maximum tube voltage of 39 kVp and the CNR of the signals in projection space as the quality metric, and concluded that higher energy spectra are beneficial in DBT.[14] Zhao *et al.* reported on a simulation study that used the SNR in projection space of a simulated microcalcification in a homogeneous breast.[73] The highest tube voltage studied was 40 kVp and the projections included in the study were 0° and 25°. They concluded that a higher SNR is achieved at mildly higher kVp settings than those used for mammography for all breasts except a very thick glandular breast, for which a 9 kVp increase was found to be beneficial. Glick *et al.* performed a simulation using a frequency domain detectability metric in projection space to study the optimal x-ray spectrum up to 40 kVp, using a serial cascaded model to introduce the system characteristics into the simulation and a homogeneous background, and found that a tungsten target/rhodium filter combination maximizes the detectability metric.[74] As opposed to the previous studies, Glick *et al.* reported that x-ray spectra at the lower mammographic energies result in the highest detectability. Wu *et al.* studied x-ray spectra optimization empirically, acquiring the 0° projections of a disk over a homogenous background and using CNR normalized by the mean glandular dose (MGD) of the signal in the projection as the quality metric.[75] In this study, higher kVp energies were found to be beneficial only for the thickest breasts.

IV.B. Total exposure optimization

In an early study that attempted to optimize the exposure levels needed in DBT, Kempston *et al.* found that signal-difference-to-noise ratio (SDNR) in structured phantoms first increases with increasing exposure and then levels off. This suggested that further increase in exposure has no benefit to

image quality due to anatomic noise becoming dominant.[76] In a study to determine the total exposure level needed to detect and characterize different types of lesions compared to mammography exposure levels, Timberg *et al.* found that results vary with lesion type, with, in general, high contrast and well defined lesions requiring half of the exposure of a single mammographic view, while low contrast lesions with diffuse edges require double the exposure of one mammogram.[77] The median exposure level was equal to that of a single mammographic exposure. Finally, no significant difference was found when using pixel binning, suggesting that this mode could be used to reduce acquisition time.

In a study that characterized a commercial DBT system (Selenia Dimensions, Hologic, Inc., Bedford, MA), Feng and Sechopoulos used breast phantoms to determine what tube voltages were selected by the automatic exposure control (AEC) for DBT and mammography, finding that for the same breast phantom thickness and composition, the AEC selects a higher tube voltage for tomosynthesis acquisition than mammography.[78] However, due to the differences in the filtration used (DBT: Al, mammography: Rh or Ag), for breast phantoms below 6 cm thick the first half value layers of the mammography spectra are higher than the first half value layers of the DBT spectra.

IV.C. Distribution of total exposure

In terms of how the available tube current-exposure time product should be divided among the projections, Nishikawa *et al.* proposed a nonuniform distribution of this technique parameter.[54] In their proposition, the authors assume that clinical tomosynthesis will be performed by acquisition of a single view [purportedly the medio-lateral oblique (MLO) view] with a tube current-exposure time product that results in double that used for a mammographic acquisition. Using this assumption, Nishikawa *et al.* proposed to assign half of the total exposure available to the central projection (0°), while dividing the other half equally among the remaining projections. This would mean that the central projection would be almost the equivalent of a mammographic acquisition. It would not be exactly equivalent to a mammographic acquisition because currently all tomosynthesis acquisitions are performed without an x-ray scatter grid, which is normally used for mammographic acquisitions. Furthermore, the authors propose that the physician use the tomosynthesis reconstructed image only for mass detection [in addition to using a computer aided detection (CADe) algorithm optimized for mass detection] and the central projection 2D image only for microcalcification detection (again in addition to using a CADe for microcalcification detection). In this way, the authors propose a method that ideally leverages the strengths of both tomosynthesis and mammography with a single acquisition and with no more dose to the breast than that currently used for a standard two view mammographic acquisition.

This proposed method was tested by Das *et al.* using mastectomy specimen-based computer simulations of breasts undergoing tomosynthesis acquisition.[55] In a localization receiver operating characteristic (LROC) study, the authors found that the observers (medical physicists) performed better with the standard DBT image (acquired using uniform distribution of total exposure among all the projections) than with the proposed half-dose central projection, but performance improved only in the detection of simulated microcalcifications. When comparing the DBT acquisitions with uniform exposure distribution with the acquisitions with variable exposure distribution as proposed by Nishikawa *et al.*, the authors did not find a statistically significant difference. Therefore, this study would suggest that performing standard DBT with a uniform exposure distribution is more preferable than the variable dose distribution approach proposed by Nishikawa *et al.* Currently, research is ongoing on the development of a synthetic mammogram from the DBT projection data, obviating the need to acquire a separate mammogram during DBT imaging (see the accompanying review paper on post-acquisition processes in DBT). It could be of interest to study how such a synthetic mammogram, once fully developed, could be incorporated into an acquisition and interpretation protocol such as the one proposed by Nishikawa *et al.*

In another study on variable dose DBT, Hu and Zhao developed a cascaded linear system model with which they implemented an ideal observer model to estimate the detectability index, d', resulting from acquisition of DBT images of microcalcifications of different sizes.[79] In addition to the uniform dose distribution, Hu and Zhao investigated two different variable dose distributions in which approximately 60% of the total exposure was used in the central five and seven projections of a total of 25 projections in a complete tomosynthesis acquisition. Although the authors also studied different values for the reconstruction algorithm's window width of the slice thickness filter (B), for a given value of B, they found that a variable exposure distribution could be beneficial only for detection of small (<200 μm) signals. In the resulting phantom image obtained (Fig. 4), an improved visibility of the microcalcifications can be seen with the variable dose acquisition.

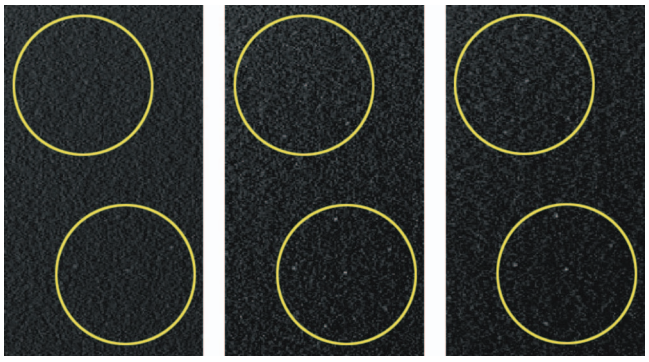

FIG. 4. Comparison of microcalcification visibility between a standard DBT acquisition (constant exposure per projection) (left), and two different variable exposure acquisition schemes (center: central 7 projections with 4× the exposure of the 18 peripheral projections; and right: central 5 projections with 4.8× the exposure of the 20 peripheral projections), showing improved visibility for the latter. The total exposure for all three acquisitions was approximately equal. Reprinted with permission from Y.-H. Hu and W. Zhao, "The effect of angular dose distribution on the detection of microcalcifications in digital breast tomosynthesis," Med. Phys. **38**(5), 2455–2466 (2011).

It should be noted that one commercial DBT system, the IMS Giotto TOMO listed in Table I, can use a variable dose distribution among its 13 projections. In this mode, 50% of the total tube output available for the entire tomosynthesis acquisition is used during acquisition of the 0° projection, while the other 50% is distributed evenly among the other 12 projections. Although this scheme is currently an option in the commercial system approved for clinical use outside the U.S., the manufacturer plans to use a constant tube output distribution only in its U.S. commercial system, once FDA approved. Furthermore, this manufacturer is investigating a prototype system in which the projections are unevenly distributed among the 40° spanned during DBT acquisition.[34]

V. RADIATION DOSE

In breast imaging, the radiation dose of concern is that deposited in the glandular tissue of the breast since this is the tissue at risk of cancer development. Therefore, the concept of the mean glandular dose (MGD) has been introduced as the metric for dose in breast imaging. In general, to estimate MGD, Monte Carlo methods that simulate the acquisition process have been used to quantify the energy deposited in the glandular portion of a breast. In these simulations, the breast is usually represented as a homogeneous adipose-glandular tissue mixture enveloped by a layer of skin.[80–85] Normally, the air kerma at the entrance surface of the breast is used as the normalizing factor for MGD, resulting in the normalized mean glandular dose (D_gN), which is expressed in units of mGy of mean glandular dose per unit mGy air kerma.

In DBT, to simplify the estimation of the total MGD from a complete acquisition, the concept of the relative glandular dose (RGD) was proposed, defined as[86]

$$\mathrm{RGD}(\alpha) = \frac{D_gN(\alpha)}{D_gN_0}, \tag{3}$$

where $D_gN(\alpha)$ and D_gN_0 are the normalized glandular dose values for projection angles α and 0°, respectively. Therefore, the latter is equivalent to the D_gN for a mammographic acquisition under the same conditions. Using the RGD, the total D_gN for a complete DBT acquisition can be computed using[86]

$$D_gN = D_gN_0 \cdot \sum_{\alpha} \mathrm{RGD}(\alpha) = D_gN_0 \cdot N_\alpha \cdot \mu_{\mathrm{RGD}}. \tag{4}$$

Where N_α is the number of projections acquired, and μ_{RGD} is the mean of the RGD of the projection angles involved in the tomosynthesis acquisition. As opposed to D_gN, RGD, and therefore, μ_{RGD}, have been shown to be a weak function of x-ray spectrum and breast glandular fraction, so polynomial fit equations for RGD as a function of breast size and compressed thickness have been published.[86] Since the European model of breast dosimetry, also used by the IAEA, only considers the CC view and a single breast size, RGD (represented as $t(\theta)$ in that publication) is only a function of compressed breast thickness, resulting in a table being published providing $t(\theta)$ for different breast thicknesses and projection angles.[87] In addition, for specific DBT system implementations where the projection angles are fixed, μ_{RGD} (T in the European model) can be reported for each breast thickness.[87] These values, combined with published data for D_gN_0 either for mammography[80–85] or specifically for DBT,[86,88,89] can be used to compute D_gN for the complete tomosynthesis acquisition.

Of course, if a tomosynthesis acquisition results in a μ_{RGD} of unity, then D_gN can be estimated simply by multiplying the appropriate D_gN_0 by the number of projections in the acquisition. For certain acquisition conditions, like small total angular ranges and for some breast sizes and thicknesses, the μ_{RGD} has been found to be very close to unity.[86,87]

The results on normalized glandular dose were used by Feng and Sechopoulos, combined with measurements of air kerma and x-ray spectra characteristics based on the automatic exposure control (AEC), to characterize the dosimetry of the Hologic Selenia Dimensions clinical DBT system.[78] Using homogeneous breast phantoms of varying glandular fraction and compressed breast thickness, the authors determined the tube voltage and tube current-exposure time product selected by the AEC to acquire a DBT and a mammography image. From this data and the corresponding D_gN and RGD values, the authors estimated the glandular dose to each breast phantom for each imaging modality. For the traditional definition of an average breast (5 cm thick, 50% glandular fraction), the authors found that DBT acquisition with this specific system results in only an 8% higher MGD than mammography, and that both are substantially lower than the dose values used recently in the clinic with previous generation digital mammography systems.[90] For a breast definition that has more recently been proposed to better represent an average breast (6 cm thick, 14.3% glandular fraction),[91] the authors found a larger dose increase of 83% from mammography to DBT. It should be noted that these findings are system-specific, and therefore these results may be different for other DBT systems from other manufacturers.

It must be noted that these values were based on using a homogeneous phantom to characterize the behavior of the AEC. In the future, once a large number of combined mammography/tomosynthesis acquisitions during one breast compression are performed in the clinical realm, a better estimation of the comparison of the dose between these two modalities for the same breasts can be performed. Of course, for such a study the true glandular fraction of each breast would not be known. However, analysis of the variation with glandular fraction of the ratio of D_gN for mammography and DBT for the same breast thickness using the data published by Feng and Sechopoulos (Tables IV and V) (Ref. 78) shows that using an incorrect glandular fraction would introduce an error that ranges from 0% to 10%, with a mean of 5%, making this type of study valid and feasible.

VI. X-RAY SCATTER

The detection and inclusion of the x-ray scatter signal in the acquired images in x-ray imaging results in a loss of contrast, among other effects such as loss of accuracy, depending on modality. In mammography, x-ray scatter has been dealt with through the use of anti-scatter grids located between the

breast and the detector, which preferentially absorb scattered x-rays and transmit primary (non-scattered) x-rays. Of course, anti-scatter grids are not perfect, and involve a penalty of increased dose to the breast to achieve the same signal at the detector.[92] In DBT, x-ray scatter is of additional concern compared to mammography for two basic reasons: (i) the varying relative position of the x-ray source compared to the detector would result in severe absorption of the primary x-rays by the grid at non-zero projection angles, and (ii) the already low exposure available per projection would be lowered further by the use of a grid. It is possible that the first limitation could be overcome with some novel design for the grid. For example, the grid lines could be oriented parallel to the x-ray tube travel direction, with the grid moving during acquisition in the perpendicular direction. However, there currently is no public information that such a grid is being used or developed. In addition, it is not clear if the second limitation mentioned above could be overcome by any novel grid design. Therefore, the magnitude, characteristics, and impact on image quality that x-ray scatter has on DBT has been studied, and new methods to reduce its impact have been sought.

In a scatter characterization study, Sechopoulos *et al.* used Monte Carlo methods to estimate the scatter PSF and scatter-to-primary ratio (SPR) for varying imaging conditions and breast definitions.[93] The authors found that the tails of the scatter PSF on the side opposite the x-ray tube location widen with increasing projection angle, while there is a narrowing of the tail on the same side as the x-ray tube location. In addition, as expected from previous mammography results,[94] the scatter PSF does not vary considerably with x-ray spectrum and varies to a small extent with breast glandular fraction. The analysis of SPR resulted in polynomial fit equations for determining SPR at the center of mass of the breast projection as a function of tomosynthesis projection angle, glandular fraction, and breast thickness. Incidentally, it was found that the breast support plate and detector cover have a substantial impact on SPR distribution, especially for thicker breasts (> 5 cm), both in mammography and DBT. This results in the highest SPR for these breasts not being located at the center of mass, as previously thought, but at the periphery of the breast.

The impact that x-ray scatter has on DBT image quality was investigated by Wu *et al.*, using analytical methods to simulate tomosynthesis images with scatter, quantum noise, and realistic breast backgrounds with added simulated lesions.[95] The authors found distinct cupping, loss of contrast, and a loss in accuracy of the reconstructed voxel values (Fig. 5). Quantitative analysis found that lesion contrast was reduced by the presence of scatter by 30%, while SDNR was reduced by 60% and the inferred attenuation coefficient was reduced by 28%. Of course, although this impact in objective terms is clear and substantial, how this affects clinical performance has not been studied.

VI.A. Scatter reduction methods

Clearly, it would be beneficial for image quality in DBT for some form of x-ray scatter reduction or correction method to be used. One such proposed method, described by Liu *et al.*, is

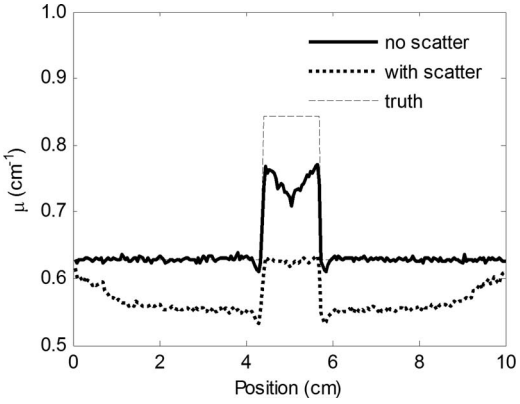

FIG. 5. Horizontal profile through the center of a lesion in a DBT reconstructed slice showing the reduction in voxel values and contrast due to the presence of x-ray scatter. Reprinted with permission from Wu *et al.*, "Evaluation of scatter effects on image quality for breast tomosynthesis," Med. Phys. **36**(10), 4425–4432 (2009). Copyright © 2009, American Association of Physicists in Medicine.

a software algorithm that involves no additional hardware.[96] In this proposed method, after reconstructing the DBT image, the voxels in the reconstructed breast are mapped to a limited number of different combinations of mixtures of adipose and glandular tissue or to calcium. The resulting classified 3D image is input into a Monte Carlo simulation to estimate the scatter signal distribution in the projections. These estimates are then subtracted from the originally acquired projections, yielding estimates of the primary only signal in each, which are used to reconstruct the breast again. The authors show that the proposed method results in an increase in voxel values and state that they found an increase in contrast. However, as expected, an increase in noise was also found. X-ray scatter correction algorithms that are based on the subtraction of the low-frequency scatter signal from the acquired projections with no reduction of the scatter quantum noise are characterized by this increase in noise by reduction of the overall signal.[96] Currently, the performance of a Monte Carlo simulation to estimate the scatter field for each acquired patient image involves many hours of computation time, making such an approach challenging to introduce for clinical work. Scatter estimation acceleration methods[98] in conjunction with the ever-increasing speed of computers could in the future make this type of approach feasible.

To avoid the computation time needed for patient-specific Monte Carlo simulations, Feng and Sechopoulos proposed to take advantage of the known insensitivity of the scatter distribution to breast size and composition to perform a model-based scatter correction.[99] Specifically, the authors propose that since scatter distribution is a weak function of these two parameters, a precomputed scatter signal distribution for simulated homogeneous breasts of similar, but not the same, size and shape as that of the acquired clinical case could provide a good estimate of the true scatter distribution in the latter. Before performing the subtraction of the model-based scatter estimate from the acquired projections, the former would have to be registered to the latter to accommodate the differences in shape. Therefore, by eliminating the need to estimate the scatter signal exactly, a limited num-

ber of Monte Carlo precomputed scatter distributions that cover the range of possible breast shapes could be stored and used. Alternatively, a multiparameter model could be developed to produce the scatter distribution estimate from a few input parameters (e.g., breast thickness, chest wall-to-nipple distance, and projection angle), without the need for computation-intensive simulations. To decrease the impact of the scatter quantum noise, the authors also propose the use of an adaptive means filter to reduce noise while attempting to preserve the spatial resolution. Using a textured breast phantom, Feng and Sechopoulos showed an improvement in signal difference, SDNR and integrated signal difference between background and lesions when applying their proposed algorithm, superior to that obtained when applying only the noise reduction filter.

VII. BREAST COMPRESSION REDUCTION

It has been proposed that since tomosynthesis inherently reduces the problem of tissue superposition, or anatomic noise, present in planar imaging, DBT could be performed with substantial reduction in the mechanical breast compression used during acquisition compared to mammography.[100,101] To investigate this possibility, Saunders *et al.* performed a study with phantom images generated using Monte Carlo methods, simulating three breasts each with two different compressed thicknesses (4 and 6 cm) and one alternate reduced compression version (4.5 and 6.75 cm).[100] Using lesion conspicuity as the metric of choice for masses and calcifications, the authors found no significant difference with the reduced compression when the exposure parameters were varied to maintain a constant dose to the breasts. Förnvik *et al.* performed a clinical study in which patient DBT images were acquired with full compression and with half of the force used during full compression, using the same acquisition technique for both acquisitions.[101] Portions of the DBT images that included different types of features, such as lesions, calcifications, glandular structures, and fibrous strands/vessels, were selected and compared. The image quality comparison, which was performed by three radiologists subjectively and independently, yielded a significant preference for the full compression image only for the visualization quality of the glandular structures and fibrous strands combined. Not surprisingly, the patient volunteers had a preference for the reduced compression acquisition.

Although minimization of tissue superposition is the main reason for breast compression in breast imaging, it is not the only one. Reduction of x-ray scatter signal, breast dose and motion artifacts, and increase in the amount of breast tissue in the field of view are other important considerations for breast compression.[102] Therefore, before DBT with reduced compression can be performed clinically, it must be determined that these other factors are not adversely affected by the reduction in compression force.

VIII. CONCLUSIONS

A lot of research has been performed on many of the acquisition parameters and other physical aspects of DBT image acquisition, such as radiation dose and x-ray scatter. In many aspects, this has resulted in a good understanding of the issues, with several different research approaches often arriving at similar conclusions. For example, it was repeatedly found that the widest angular ranges (approx. 45°–60°) studied resulted in increased image quality, while the optimal number of projections was achieved at a relatively low number (approx. 15–20). Other aspects, e.g., a correction or reduction of the x-ray scatter signal in DBT projections, still necessitate further research before application in clinical DBT imaging.

ACKNOWLEDGMENTS

The work by the author's group discussed here has been supported by the Atlanta Clinical and Translational Science Institute, the University Research Committee of Emory University, the National Science Foundation (DMS-1115627), the National Cancer Institute (R01CA163746, P50CA128301), and the National Center for Research Resources (UL1RR025008). The content is solely the responsibility of the author and does not necessarily represent the official views of these institutions. The author would like to thank Dr. Cedric Yu, Dr. Wei Zhao, and Dr. Martin Yaffe for giving permission to reprint their figures, Dr. James Nagy and Steve Feng for scientific input and Jessica Paulishen for assistance with editing.

[a]Author to whom correspondence should be addressed. Electronic mail: isechop@emory.edu; Telephone: (404)712-2412; Fax: (404)712-5813.

[1]NCI-funded Breast Cancer Surveillance Consortium co-operative agreement, "Performance Measures for 1,960,150 Screening Mammography Examinations from 2002 to 2006 by Age - based on BCSC data as of 2009," November 15, 2011 [accessed April 26, 2012]; Available from: http://breastscreening.cancer.gov/data/performance/screening/2009/perf_age.html.

[2]K. Kerlikowske, D. Grady, J. Barclay, E. A. Sickles, and V. Ernster, "Effect of age, breast density, and family history on the sensitivity of first screening mammography," JAMA, J. Am. Med. Assoc. **276**, 33–38 (1996).

[3]P. A. Carney, D. L. Miglioretti, B. C. Yankaskas, K. Kerlikowske, R. Rosenberg, C. M. Rutter, B. M. Geller, L. A. Abraham, S. H. Taplin, M. Dignan, G. Cutter, and R. Ballard-Barbash, "Individual and combined effects of age, breast density, and hormone replacement therapy use on the accuracy of screening mammography," Ann. Intern Med. **138**, 168–175 (2003).

[4]J. M. Boone, T. R. Nelson, K. K. Lindfors, and J. A. Seibert, "Dedicated breast CT: Radiation dose and image quality evaluation," Radiology **221**, 657–667 (2001).

[5]R. Ning, D. L. Conover, B. Chen, L. Schiffhauer, J. Cullinan, Y. Ning, and A. E. Robinson, "Flat-panel-detector-based cone-beam volume CT breast imaging: Phantom and specimen study," Proc. SPIE **4682**, 218–227 (2002).

[6]B. Chen and R. Ning, "Cone-beam volume CT breast imaging: Feasibility study," Med. Phys. **29**, 755–770 (2002).

[7]R. L. McKinley, M. P. Tornai, E. Samei, and M. L. Bradshaw, "Initial study of quasi-monochromatic x-ray beam performance for x-ray computed mammotomography," IEEE Trans. Nucl. Sci. **52**, 1243–1250 (2005).

[8]R. L. McKinley, M. P. Tornai, C. Brzymialkiewicz, P. Madhav, E. Samei, and J. E. Bowsher, "Analysis of a novel offset cone-beam computed mammotomography system geometry for accomodating various breast sizes," Phys. Med. **21**, 48–55 (2006).

[9]K. K. Lindfors, J. M. Boone, T. R. Nelson, K. Yang, A. L. C. Kwan, and D. F. Miller, "Dedicated breast CT: Initial clinical experience," Radiology **246**, 725–733 (2008).

[10]W. Kalender, M. Beister, J. Boone, D. Kolditz, S. Vollmar, and M. Weigel, "High-resolution spiral CT of the breast at very low dose: Concept and feasibility considerations," Eur. Radiol. **22**, 1–8 (2012).

[11]J. T. Dobbins III and D. J. Godfrey, "Digital x-ray tomosynthesis: Current state of the art and clinical potential," Phys. Med. Biol. **48**, R65–R106 (2003).
[12]J. T. Dobbins III, "Tomosynthesis imaging: At a translational crossroads," Med. Phys. **36**, 1956–1967 (2009).
[13]L. T. Niklason *et al.*, "Digital tomosynthesis in breast imaging," Radiology **205**, 399–406 (1997).
[14]B. Ren, C. Ruth, J. Stein, A. Smith, I. Shaw, and Z. Jing, "Design and performance of the prototype full field breast tomosynthesis system with selenium based flat panel detector," Proc. SPIE **5745**, 550–561 (2005).
[15]J. W. Eberhard *et al.*, "High-speed large-angle mammography tomosynthesis system," Proc. SPIE **6142**, 61420C (2006).
[16]J. A. Baker and J. Y. Lo, "Breast tomosynthesis: State-of-the-art and review of the literature," Acad. Radiol. **18**, 1298–1310 (2011).
[17]B. Ren, C. Ruth, T. Wu, Y. Zhang, A. Smith, L. Niklason, C. Williams, E. Ingal, B. Polischuk, and Z. Jing, "A new generation FFDM/tomosynthesis fusion system with selenium detector," Proc. SPIE **7622**, 76220B (2010).
[18]J. Zhou, B. Zhao, and W. Zhao, "A computer simulation platform for the optimization of a breast tomosynthesis system," Med. Phys. **34**, 1098–1109 (2007).
[19]X. Qian, R. Rajaram, X. Calderon-Colon, G. Yang, T. Phan, D. S. Lalush, J. Lu, and O. Zhou, "Design and characterization of a spatially distributed multibeam field emission x-ray source for stationary digital breast tomosynthesis," Med. Phys. **36**, 4389–4399 (2009).
[20]F. Sprenger, X. Calderon-Colon, Y. Cheng, K. Englestad, J. Lu, J. Maltz, A. Paidi, X. Qian, D. Spronk, S. Sultana, G. Yang, and O. Zhou, "Distributed source x-ray tube technology for tomosynthesis imaging," Proc. SPIE **7622**, 76225M (2010).
[21]F. Sprenger, X. Calderon, E. Gidcumb, J. Lu, X. Qian, D. Spronk, A. Tucker, G. Yang, and O. Zhou, "Stationary digital breast tomosynthesis with distributed field emission x-ray tube," Proc. SPIE **7961**, 79615I (2011).
[22]G. Yang, X. Qian, T. Phan, F. Sprenger, S. Sultana, X. Calderon-Colon, B. Kearse, D. Spronk, J. Lu, and O. Zhou, "Design and feasibility studies of a stationary digital breast tomosynthesis system," Nucl. Instrum. Methods Phys. Res. A **648**, S220–S223 (2011).
[23]X. Qian, A. Tucker, E. Gidcumb, J. Lu, O. Zhou, D. Spronk, F. Sprenger, Y. Zhang, D. Kennedy, T. Farbizio, and Z. Jing, "A stationary digital breast tomosynthesis scanner," Proc. SPIE **8313**, 831352 (2012).
[24]A. Tucker, X. Qian, E. Gidcumb, D. Spronk, F. Sprenger, J. Kuo, S. Ng, J. Lu, and O. Zhou, "Optimizing configuration parameters of a stationary digital breast tomosynthesis system based on carbon nanotube x-ray sources," Proc. SPIE **8313**, 831307–831310 (2012).
[25]X. Qian *et al.*, "High resolution stationary digital breast tomosynthesis using distributed carbon nanotube x-ray source array," Med. Phys. **39**, 2090–2099 (2012).
[26]F. F. Schmitzberger, E. M. Fallenberg, R. Lawaczeck, M. Hemmendorff, E. Moa, M. Danielsson, U. Bick, S. Diekmann, A. Pollinger, F. J. Engelken, and F. Diekmann, "Development of low-dose photon-counting contrast-enhanced tomosynthesis with spectral imaging," Radiology **259**, 558–564 (2011).
[27]M. G. Wallis, E. Moa, F. Zanca, K. Leifland, and M. Danielsson, "Two-view and single-view tomosynthesis versus full-field digital mammography: High-resolution x-ray imaging observer study," Radiology **262**, 788–796 (2012).
[28]M. Aslund, B. Cederstrom, M. Lundqvist, and M. Danielsson, "Scatter rejection in multislit digital mammography," Med. Phys. **33**, 933–940 (2006).
[29]A. Maidment *et al.*, "Evaluation of a photon-counting breast tomosynthesis imaging system," Proc. SPIE **5745**, 572–582 (2005).
[30]A. Maidment *et al.*, "Evaluation of a photon-counting breast tomosynthesis imaging system," Proc. SPIE **6142**, 61420B (2006).
[31]Presentation from the GE Healthcare representative at the 2011 AAPM tomosynthesis subcommittee meeting in Vancouver, Canada, on July 31, 2011.
[32]S. Vecchio, A. Albanese, P. Vignoli, and A. Taibi, "A novel approach to digital breast tomosynthesis for simultaneous acquisition of 2D and 3D images," Eur. Radiol. **21**, 1207–1213 (2011).
[33]R. Girometti, C. Zuiani, A. Taibi, S. Vecchio, R. Fazzin, and M. Bazzocchi, "Diagnostic yield of digital breast tomosynthesis (DBT) vs digital mammography (DM) in assessing breast cancer: A study on surgical specimens," European Congress of Radiology, Vienna, Austria, 2012.
[34]A. Albanese (personal communication, 2012).
[35]IMS Giotto, "Giotto breast tomosynthesis," http://www.imsitaly.com/downloads/IMS-Tomosynthesis-new.pdf. Last accessed September 10, 2012.
[36]E. Fredenberg, M. Lundqvist, M. Aslund, M. Hemmendorff, B. Cederstrom, and M. Danielsson, "A photon-counting detector for dual-energy breast tomosynthesis," Proc. SPIE **7258**, 72581J (2009).
[37]P. Strömmer (personal communication, 2012).
[38]S. Young, S. Park, S. K. Anderson, A. Badano, K. J. Myers, and P. Bakic, "Estimating breast tomosynthesis performance in detection tasks with variable-background phantoms," Proc. SPIE **7258**, 72580O–72589O (2009).
[39]E. Shaheen, C. Van Ongeval, F. Zanca, L. Cockmartin, N. Marshall, J. Jacobs, K. C. Young, D. R. Dance, and H. Bosmans, "The simulation of 3D microcalcification clusters in 2D digital mammography and breast tomosynthesis," Med. Phys. **38**, 6659–6671 (2011).
[40]T. Mertelmeier (personal communication, 2012).
[41]J. G. Mainprize, X. Wang, and M. J. Yaffe, "The effect of lag on image quality for a digital breast tomosynthesis system," Proc. SPIE **7258**, 72580R–72581R (2009).
[42]M. Bissonnette *et al.*, "Digital breast tomosynthesis using an amorphous selenium flat panel detector," Proc. SPIE **5745**, 529–540 (2005).
[43]B. Zhao and W. Zhao, "Imaging performance of an amorphous selenium digital mammography detector in a breast tomosynthesis system," Med. Phys. **35**, 1978–1987 (2008).
[44]L. K. Cheung, Z. Jing, S. Bogdanovich, K. Golden, S. Robinson, E. Beliaevskaia, and S. Parikh, "Image performance of a new amorphous selenium flat panel x-ray detector designed for digital breast tomosynthesis," Proc. SPIE **5745**, 1282–1290 (2005).
[45]J. G. Mainprize, A. K. Bloomquist, M. P. Kempston, and M. J. Yaffe, "Resolution at oblique incidence angles of a flat panel imager for breast tomosynthesis," Med. Phys. **33**, 3159–3164 (2006).
[46]M. Freed, S. Park, and A. Badano, "A fast, angle-dependent, analytical model of CsI detector response for optimization of 3D x-ray breast imaging systems," Med. Phys. **37**, 2593–2605 (2010).
[47]R. Acciavatti and A. Maidment, "Calculation of OTF, NPS, and DQE for oblique x-ray incidence on turbid granular phosphors," in *Proceedings of the 10th International Workshop on Digital Mammography* (Springer Berlin Heidelberg, Girona, Spain, 2010), pp. 436–443.
[48]R. J. Acciavatti and A. Maidment, "Optimization of phosphor-based detector design for oblique x-ray incidence in digital breast tomosynthesis," Med. Phys. **38**, 6188–6202 (2011).
[49]A. Badano, I. S. Kyprianou, R. J. Jennings, and J. Sempau, "Anisotropic imaging performance in breast tomosynthesis," Med. Phys. **34**, 4076–4091 (2007).
[50]A. Badano, M. Freed, and Y. Fang, "Oblique incidence effects in direct x-ray detectors: A first-order approximation using a physics-based analytical model," Med. Phys. **38**, 2095–2098 (2011).
[51]I. S. Reiser, R. M. Nishikawa, and B. A. Lau, "Effect of non-isotropic detector blur on microcalcification detectability in tomosynthesis," Proc. SPIE **7258**, 72585Z (2009).
[52]J. Chen, J. Lehnert, P. O'Connor, G. D. Geronimo, E. Dolazza, O. Tousignant, L. Laperrière, J. Greenspan, and W. Zhao, "Feasibility of amorphous selenium based photon counting detectors for digital breast tomosynthesis," Proc. SPIE **7258**, 72581G (2009).
[53]S. Naday, E. Bullard, S. Gunn, J. Brodrick, E. O'Tuairisg, A. McArthur, H. Amin, M. Williams, P. Judy, and A. Konstantinidis, "Optimised breast tomosynthesis with a novel CMOS flat panel detector," in *Proceedings of the 10th International Workshop on Digital Mammography* (Springer Berlin Heidelberg, Girona, Spain, 2010), pp. 428–435.
[54]R. M. Nishikawa, I. Reiser, P. Seifi, and C. J. Vyborny, "A new approach to digital breast tomosynthesis for breast cancer screening," Proc. SPIE **6510**, 65103C–65108C (2007).
[55]M. Das, H. C. Gifford, J. M. O'Connor, and S. J. Glick, "Evaluation of a variable dose acquisition technique for microcalcification and mass detection in digital breast tomosynthesis," Med. Phys. **36**, 1976–1984 (2009).
[56]B. Ren, T. Wu, A. Smith, C. Ruth, L. Niklason, Z. Jing, and J. Stein, "The dependence of tomosynthesis imaging performance on the number of scan projections," in *Proceedings of the 8th International Workshop on Digital Mammography* (Springer Berlin Heidelberg, Manchester, 2006), pp. 517–524.

[57]T. Wu, R. H. Moore, E. A. Rafferty, and D. B. Kopans, "A comparison of reconstruction algorithms for breast tomosynthesis," Med. Phys. **31**, 2636–2647 (2004).
[58]Y.-H. Hu, B. Zhao, and W. Zhao, "Image artifacts in digital breast tomosynthesis: Investigation of the effects of system geometry and reconstruction parameters using a linear system approach," Med. Phys. **35**, 5242–5252 (2008).
[59]T. Mertelmeier, J. Ludwig, B. Zhao, and W. Zhao, "Optimization of tomosynthesis acquisition parameters: angular range and number of projections," in *Proceedings of the 9th International Workshop on Digital Mammography* (Springer Berlin Heidelberg, Tucson, AZ, 2008), pp. 220–227.
[60]I. Sechopoulos and C. Ghetti, "Optimization of the acquisition geometry in digital tomosynthesis of the breast," Med. Phys. **36**, 1199–1207 (2009).
[61]A. S. Chawla, E. Samei, R. Saunders, J. Lo, and J. A. Baker, "A mathematical model platform for optimizing a multiprojection breast imaging system," Med. Phys. **35**, 1337–1345 (2008).
[62]A. S. Chawla, J. Y. Lo, J. A. Baker, and E. Samei, "Optimized image acquisition for breast tomosynthesis in projection and reconstruction space," Med. Phys. **36**, 4859–4869 (2009).
[63]H. C. Gifford, C. S. Didier, M. Das, and S. J. Glick, "Optimizing breast-tomosynthesis acquisition parameters with scanning model observers," Proc. SPIE **6917**, 69170S–69171S (2008).
[64]I. Reiser and R. M. Nishikawa, "Task-based assessment of breast tomosynthesis: Effect of acquisition parameters and quantum noise," Med. Phys. **37**, 1591–1600 (2010).
[65]Y. Lu, H. Chan, J. Wei, M. Goodsitt, P. L. Carson, L. Hadjiiski, A. Schmitz, J. W. Eberhard, and B. E. Claus, "Image quality of microcalcifications in digital breast tomosynthesis: Effects of projection-view distributions," Med. Phys. **38**, 5703–5712 (2011).
[66]D. Van de Sompel, S. M. Brady, and J. Boone, "Task-based performance analysis of FBP, SART and ML for digital breast tomosynthesis using signal CNR and channelised hotelling observers," Med. Image Anal. **15**, 53–70 (2011).
[67]B. Ren, C. Ruth, Y. Zhang, A. Smith, C. Williams, B. Polischuk, and Z. Jing, "The CNR method in scan angle optimization of tomosynthesis and its limitations," Proc. SPIE **7258**, 72585W (2009).
[68]G. J. Gang, D. J. Tward, J. Lee, and J. H. Siewerdsen, "Anatomical background and generalized detectability in tomosynthesis and cone-beam CT," Med. Phys. **37**, 1948–1965 (2010).
[69]G. M. Stevens, R. L. Birdwell, C. F. Beaulieu, D. M. Ikeda, and N. J. Pelc, "Circular tomosynthesis: potential in imaging of breast and upper cervical spine–preliminary phantom and in vitro study," Radiology **228**, 569–575 (2003).
[70]K. Zeng, H. Yu, S. Zhao, L. L. Fajardo, C. Ruth, Z. Jing, and G. Wang, "Digital tomosynthesis aided by low-resolution exact computed tomography," J. Comput. Assist. Tomogr. **31**, 976–983 (2007).
[71]D. Xia, S. Cho, J. Bian, E. Y. Sidky, C. A. Pelizzari, and X. Pan, "Tomosynthesis with source positions distributed over a surface," Proc. SPIE **6913**, 69132A–69137A (2008).
[72]J. Zhang and C. Yu, "A novel solid-angle tomosynthesis (SAT) scanning scheme," Med. Phys. **37**, 4186–4192 (2010).
[73]W. Zhao, R. Deych, and E. Dolazza, "Optimization of operational conditions for direct digital mammography detectors for digital tomosynthesis," Proc. SPIE **5745**, 1272–1281 (2005).
[74]S. J. Glick and X. Gong, "Optimal spectra for indirect detector breast tomosynthesis," Proc. SPIE **6142**, 61421L–61429L (2006).
[75]T. Wu, B. Liu, R. Moore, and D. Kopans, "Optimal acquisition techniques for digital breast tomosynthesis screening," Proc. SPIE **6142**, 61425E (2006).
[76]M. Kempston, J. Mainprize, and M. Yaffe, "Evaluating the effect of dose on reconstructed image quality in digital tomosynthesis," in *Proceedings of the 8th International Workshop on Digital Mammography* (Springer Berlin Heidelberg, Manchester, 2006), pp. 490–497.
[77]P. Timberg, M. Båth, I. Andersson, T. Svahn, M. Ruschin, B. Hemdal, S. Mattsson, and A. Tingberg, "Impact of dose on observer performance in breast tomosynthesis using breast specimens," Proc. SPIE **6913**, 69134J (2008).
[78]S. S. J. Feng and I. Sechopoulos, "Clinical digital breast tomosynthesis system: Dosimetric characterization," Radiology **263**, 35–42 (2012).
[79]Y.-H. Hu and W. Zhao, "The effect of angular dose distribution on the detection of microcalcifications in digital breast tomosynthesis," Med. Phys. **38**, 2455–2466 (2011).
[80]D. R. Dance, "Monte Carlo calculation of conversion factors for the estimation of mean glandular breast dose," Phys. Med. Biol. **35**, 1211–1219 (1990).
[81]X. Wu, G. T. Barnes, and D. M. Tucker, "Spectral dependence of glandular tissue dose in screen-film mammography," Radiology **179**, 143–148 (1991).
[82]X. Wu, E. L. Gingold, G. T. Barnes, and D. M. Tucker, "Normalized average glandular dose in molybdenum target-rhodium filter and rhodium target-rhodium filter mammography," Radiology **193**, 83–89 (1994).
[83]J. M. Boone, "Glandular breast dose for monoenergetic and high-energy x-ray beams: Monte Carlo assessment," Radiology **213**, 23–37 (1999).
[84]D. R. Dance, A. K. Thilander, M. Sandborg, C. L. Skinner, I. A. Castellano, and G. A. Carlsson, "Influence of anode/filter material and tube potential on contrast, signal-to-noise ratio and average absorbed dose in mammography: A Monte Carlo study," Br. J. Radiol. **73**, 1056–1067 (2000).
[85]J. M. Boone, "Normalized glandular dose (DgN) coefficients for arbitrary x-ray spectra in mammography: Computer-fit values of Monte Carlo derived data," Med. Phys. **29**, 869–875 (2002).
[86]I. Sechopoulos, S. Suryanarayanan, S. Vedantham, C. D'Orsi, and A. Karellas, "Computation of the glandular radiation dose in digital tomosynthesis of the breast," Med. Phys. **34**, 221–232 (2007).
[87]D. R. Dance, K. C. Young, and R. E. van Engen, "Estimation of mean glandular dose for breast tomosynthesis: Factors for use with the UK, European and IAEA breast dosimetry protocols," Phys. Med. Biol. **56**, 453–471 (2011).
[88]I. Sechopoulos and C. J. D'Orsi, "Glandular radiation dose in tomosynthesis of the breast using tungsten targets," J. Appl. Clin. Med. Phys. **9**, 161–171 (2008).
[89]A. K. W. Ma, D. G. Darambara, A. Stewart, S. Gunn, and E. Bullard, "Mean glandular dose estimation using MCNPX for a digital breast tomosynthesis system with tungsten/aluminum and tungsten/aluminum + silver x-ray anode-filter combinations," Med. Phys. **35**, 5278–5289 (2008).
[90]R. E. Hendrick, E. D. Pisano, A. Averbukh, C. Moran, E. A. Berns, M. J. Yaffe, B. Herman, S. Acharyya, and C. Gatsonis, "Comparison of acquisition parameters and breast dose in digital mammography and screen-film mammography in the American College of Radiology Imaging Network digital mammographic imaging screening trial," Am. J. Roentgenol. **194**, 362–369 (2010).
[91]M. J. Yaffe, J. M. Boone, N. Packard, O. Alonzo-Proulx, S. Y. Huang, C. L. Peressotti, A. Al-Mayah, and K. Brock, "The myth of the 50-50 breast," Med. Phys. **36**, 5437–5443 (2009).
[92]P. S. Rezentes, A. de Almeida, and G. T. Barnes, "Mammography grid performance," Radiology **210**, 227–232 (1999).
[93]I. Sechopoulos, S. Suryanarayanan, S. Vedantham, C. J. D'Orsi, and A. Karellas, "Scatter radiation in digital tomosynthesis of the breast," Med. Phys. **34**, 564–576 (2007).
[94]J. M. Boone, K. K. Lindfors, V. N. Cooper III, and J. A. Seibert, "Scatter/primary in mammography: Comprehensive results," Med. Phys. **27**, 2408–2416 (2000).
[95]G. Wu, J. G. Mainprize, J. M. Boone, and M. J. Yaffe, "Evaluation of scatter effects on image quality for breast tomosynthesis," Med. Phys. **36**, 4425–4432 (2009).
[96]B. Liu, T. Wu, R. H. Moore, and D. B. Kopans, "Monte Carlo simulation of x-ray scatter based on patient model from digital breast tomosynthesis," Proc. SPIE **6142**, 61421N–61429N (2006).
[97]L. Zhu, J. Wang, and L. Xing, "Noise suppression in scatter correction for cone-beam CT," Med. Phys. **36**, 741–752 (2009).
[98]A. P. Colijn and F. J. Beekman, "Accelerated simulation of cone beam x-ray scatter projections," IEEE Trans. Med. Imaging **23**, 584–590 (2004).
[99]S. S. J. Feng and I. Sechopoulos, "A software-based x-ray scatter correction method for breast tomosynthesis," Med. Phys. **38**, 6643–6653 (2011).
[100]R. S. Saunders, E. Samei, J. Y. Lo, and J. A. Baker, "Can compression be reduced for breast tomosynthesis? Monte Carlo study on mass and microcalcification conspicuity in tomosynthesis," Radiology **251**, 673–682 (2009).
[101]D. Förnvik, I. Andersson, T. Svahn, P. Timberg, S. Zackrisson, and A. Tingberg, "The effect of reduced breast compression in breast tomosynthesis: human observer study using clinical cases," Radiat. Prot. Dosim. **139**, 118–123 (2010).
[102]D. B. Kopans, *Breast Imaging*, 3rd ed. (Lippincott, Baltimore, MD, 2007).